Dielectric Properties of High-κ Oxides: Theory and Experiment for Lu_2O_3

Emiliano Bonera, Giovanna Scarel, and Marco Fanciulli

Laboratorio Nazionale Materiali e Dispositivi per la Microelettronica MDM-INFM, via Olivetti 2, 20041 Agrate Brianza (MI), Italy

Pietro Delugas and Vincenzo Fiorentini

INFM-SLACS, Sardinian Laboratory for Computational Materials Science, and Department of Physics, University of Cagliari, Cittadella Universitaria, 09042 Monserrato (CA), Italy

(Received 4 September 2004; published 19 January 2005)

We present a combined experimental and theoretical analysis of the dielectric and vibrational properties of crystalline lutetium oxide in its ground-state bixbyite structure. The vibrational dielectric function of Lu_2O_3 thin films grown by atomic-layer deposition was studied by infrared transmission and reflection-absorption spectroscopies, selectively accessing transverse and longitudinal optical frequencies. The static dielectric constant is extracted analyzing the infrared response. We also present first-principles density-functional linear-response calculations, which are in close agreement with experiment, and provide insight into the microscopic nature of vibrational spectra and dielectric properties.

DOI: 10.1103/PhysRevLett.94.027602 PACS numbers: 77.22.–d, 61.66.–f, 63.20.–e, 78.30.–j

The relentless demand for increased performance of Si-based microelectronic devices calls for ever decreasing device sizes. This downscaling process has led to the need to replace SiO_2 as a dielectric insulating material for gate electrodes, one of the key ingredients of the metal-insulator-semiconductor transistor, the basic building block of microelectronics. Size downscaling indeed requires a progressive decrease of the dielectric thickness of this insulating layer, d/ε_0, with d the physical thickness and ε_0 the static dielectric constant, frequently indicated also with κ. Because of its small dielectric constant, SiO_2 as a gate insulator has reached a physical thickness of 1–2 nm. With this thickness a high leakage current, due to direct tunneling, compromises the oxide functionality.

A possible solution to this problem is to reduce d/ε_0 adopting a material with a dielectric constant significantly higher than SiO_2, thus avoiding extreme reductions of the physical thickness. The quest for a dielectric for the replacement of silica in Si-based devices has focused the attention of the scientific community on the class of high-κ insulators [1,2]. Besides their technological relevance these materials pose intriguing basic questions, among them the nature and origin of their large dielectric constant. In this Letter, we unfold the physical origin of the high ε_0 and its direct connection with lattice dynamics and polarizability in these materials, analyzing the specific case of Lu_2O_3. Our work develops linking the experimentally determined infrared dielectric function $\varepsilon(\omega)$ with first-principles linear-response calculations, correlating the macroscopic electrodynamical response with an atomic-scale quantum-mechanical description. The results are eventually generalized for other high-κ oxides with the same two to three stoichiometric ratio.

Lu_2O_3 films were grown by atomic-layer deposition (ALD) at a growth temperature of 370 °C [3]. Each single growth cycle consisted of separate pulses of (i) a bis-cyclopentadienyl-Lu compound as a precursor of Lu [3] (duration: 11 s); (ii) N_2 for purging (8 s); (iii) H_2O as O precursor (11 s); (iv) N_2 to purge again (8 s). The cycle was repeated 1600 times. Since the as-grown film was amorphous, we induced crystallization by annealing at 650 °C for 30 s in N_2. The film thickness and the surface roughness were determined by x-ray reflectivity to be $d = 41$ nm and $\sigma = 1$ nm, respectively. The film was polycrystalline with randomly oriented grains having the bixbyite structure as determined by x-ray diffraction. Within the same deposition run, we grew the film both on Si and on metal substrates for transmission and reflection-absorption experiments, respectively. The Si substrate was a 0.5 mm thick wafer covered with a 1 nm thick chemical SiO_2 layer. We chose an orange-peel back (roughness ~ 5 μm) to reduce the effects of interference in transmission experiments. The metal substrate was a 50 nm thick cobalt disilicide layer grown by solid-state reaction of a Co layer on Si at 725 °C.

The infrared response was determined through Fourier-transform infrared spectroscopy [4] with a Bruker IFS66v/s spectrometer operating in a 1 mbar vacuum to remove air-related absorption bands. The experimental far-infrared (FIR) configuration (50–600 cm^{-1}) employed a mylar beam splitter, whereas the midinfrared (MIR) configuration (400–1000 cm^{-1}) was based on a KBr splitting element. The detector was a DTGS pyroelectric bolometer. Polarization was achieved with a Specac GS12000 holographic polarizer, guaranteeing a degree of polarization better than 95% for $\omega > 250$ cm^{-1}.

Structural parameters, vibrational frequencies, oscillator strengths, effective charges, electronic dielectric constants, and phonon eigenvectors (full details will be presented elsewhere) were calculated within density-functional perturbation theory (DFPT) [5] in the local-density approximation. We used the ABINIT code [6], with custom-made

norm conserving pseudopotentials for both Lu and O, k summations on a (222) mesh and an 80 Ryd energy cutoff for the plane-wave basis. From convergence studies we estimate an ~ 10 cm^{-1} error bar on predicted frequencies. The ground-state structure of Lu_2O_3 is cubic bixbyite, with a 40-atom primitive cell, space group Ia-3. Its calculated lattice constant 10.385 Å compares well with the measured bulk value [7] of 10.391 Å and is slightly higher than 10.34 Å measured on ALD-grown thin films [3]. The structure supports 16 IR-active threefold degenerate T_u modes.

Figure 1 shows the infrared transmission spectra of Lu_2O_3 for various incidence angles ϕ. In the normal ($\phi = 0°$) transmission spectrum reported in (a), the radiation is s polarized, and only TO frequencies are detectable. Transmission spectroscopy is advantaged over other experimental geometries because the film thickness negligibly affects the band position [8]. The spectrum was fitted via spectral simulation (SS) using the model of superposition of classical oscillators, as described by the equation

$$\varepsilon = \varepsilon_\infty + \varepsilon_L = \varepsilon_\infty + \sum_j S_j \frac{\omega_{\mathrm{TO}j}^2}{\omega_{\mathrm{TO}j}^2 - i\gamma_{\mathrm{TO}j}\omega - \omega^2}, \quad (1)$$

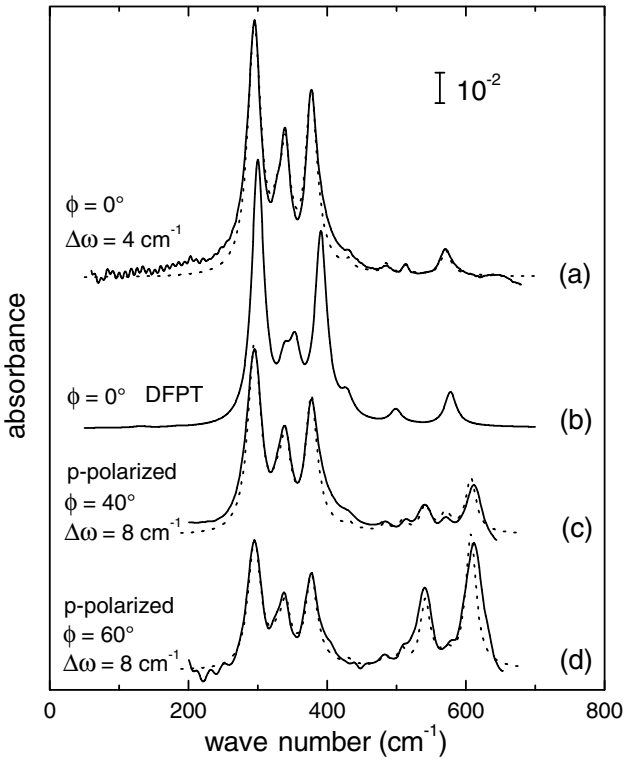

FIG. 1. (a)–(d) Transmission spectra of Lu_2O_3 on Si (solid lines). (a),(c),(d) Experimental spectra for different ϕ. (b) Normal transmission spectrum from density-functional perturbation theory (see text). All the experiments were in the far-infrared configuration. The resolution $\Delta\omega$ is shown to the left of each spectrum. The dotted lines are the spectral simulations.

where $\omega_{\mathrm{TO}j}$, $\gamma_{\mathrm{TO}j}$, and S_j are the frequency, the damping constant, and the oscillator strength of the jth oscillator. Polycrystallinity and cubic structure ensure an isotropic behavior of the dielectric function. S_j indicates the average of the total strength of the jth triplet, $S_j = 3\langle \mathbf{S}_j^{1,2,\text{ or }3} \rangle = \mathrm{Tr}\{\mathbf{S}_j^{1,2,\text{ or }3}\}$. Optical effects in the experimental spectra were taken into account in the SS with the Fresnel solution to the problem of multilayer absorption in the form derived by Hansen [9].

In Table I the parameters extracted from the experimental results are compared with those determined by DFPT. The agreement can be pictorially represented inserting in the SS algorithm the values from DFPT and assigning to each γ_j the arbitrary value of 20 cm^{-1}, Fig. 1(b). For wave numbers below 200 cm^{-1}, a set of low-intensity modes is predicted (modes TO1 to TO7), but not detected for an insufficient signal-to-noise (s/n) ratio. Interference fringes appear in this spectral region as the wavelength λ is larger than the roughness of the backsurface of the wafer, which therefore acts as an etalon mirror [8]. The fringes are not present in other FIR experiments because of the reduced instrumental resolution.

The experimental and theoretical TO spectra are in close agreement, within 5% in the determination of the energy. The strengths of the two most intense modes, which are responsible for the 80% of the value of the lattice dielectric constant ε_L, are also in a similar range of agreement. This is nontrivial from the theoretical viewpoint, as the intensities are determined by anisotropies in the dynamical Born charges which can be accessed only from first principles. Modes TO8 and TO12 exhibit a neat single-oscillator behavior, whereas the band around 330 cm^{-1} is a super-

TABLE I. TO parameters from first-principles calculations and from the SS fit of the normal transmission spectrum.

Mode	Theory		Experiment		
Label	$\omega_{\mathrm{TO}j}$ (cm^{-1})	S_j	$\omega_{\mathrm{TO}j}$ (cm^{-1})	S_j	$\gamma_{\mathrm{TO}j}$ (cm^{-1})
TO1	86	0.04	···	···	···
TO2	114	<0.01	···	···	···
TO3	125	0.05	···	···	···
TO4	132	0.07	···	···	···
TO5	145	<0.01	···	···	···
TO6	183	0.03	···	···	···
TO7	218	<0.01	···	···	···
TO8	300	4.28	295	4.6	22
TO9	339	0.53	328	0.4	18
TO10	354	0.67	340	1.1	17
TO11	374	0.03	···	···	···
TO12	391	1.74	377	1.7	20
TO13	428	0.15	431	<0.1	10
TO14	499	0.08	485	<0.1	10
TO15	526	<0.01	512	<0.1	12
TO16	578	0.14	571	0.1	17

position of TO9 and TO10, as predicted theoretically. TO12 shadows TO11 as the latter is 2 orders of magnitude less intense. TO13 is also very weak, but can be detected because it is more isolated. The observed modes TO14 and TO16 are similar to the calculated ones. Although predicted to be very weak, TO15 is in fact detectable experimentally. All TO bands drop in intensity as $E_{\parallel}$, the component of the electric field parallel to the sample surface, diminishes in non-normal incident radiation experiments, Figs. 1(c) and 1(d).

From the polar character of the material, one expects a sizable separation of TO and LO frequencies. In transmission experiments, the Berreman effect allows the direct observation of LO frequencies in thin films [10]. In the wave number range considered in this Letter, $50 < \omega < 700\ \mathrm{cm}^{-1}$, the condition $\lambda \gg d$ for the manifestation of the Berreman effect is widely satisfied. The transmission spectra collected at non-normal angles with p-polarized radiation, Figs. 1(c) and 1(d), show other bands increasing with $E_{\perp}$, the orthogonal component of the electric field. The bands observed at 539 (LO1) and 611 cm^{-1} (LO2) are related to the main LO frequencies and are consistent with the calculated values predicted at 542 and 622 cm^{-1}. The parameters extracted from the SS of Fig. 1(a) reproduce satisfactorily the off-normal transmission experiments when setting $\varepsilon_{\infty} = 4$.

In general, due to mode coupling [11], the LO eigenvectors are linear combinations of all TO eigenvectors; i.e., a LO mode cannot be related unambiguously to a single TO mode. Their relationship can be quantified projecting the LO mode onto all TO modes. For example, the most intense LO2 mode has projections 0.75, 0.40, 0.38, and 0.19 on TO16, TO12, TO8, and TO14, respectively, which account for 90% of the eigenvector norm. The other main mode LO1 has projections 0.65, 0.36, 0.40, and 0.37 (85% of the norm) on the same TO modes. All other calculated LO modes are much weaker and each of them can be identified as deriving, for 90% of the norm, from a single TO mode very close in energy (within 10 cm^{-1}).

The LO spectrum can be isolated from the TO spectrum with reflection-absorption experiments if the thin film is on a metal substrate. In the limit of extremely thin films and perfectly conductive metals, $E_{\parallel}$ is quenched and the TO bands are completely removed from the spectrum. Figure 2(a) shows the spectrum in units of reflection absorbance, defined as the logarithmic ratio between the reflectance of the reference and of the sample. As the LO frequencies are expected for $\omega > 400\ \mathrm{cm}^{-1}$, we preferred a MIR configuration for better s/n ratio and resolution. The SS is also reported superimposed to the experimental results [12]. Partial discrepancy is ascribed to the noncomplete collimation of the beam in the reflection experimental setup. The bands previously observed in off-normal transmission are isolated and exhibit slightly higher frequencies (541 and 613 cm^{-1}). This feature is typical of

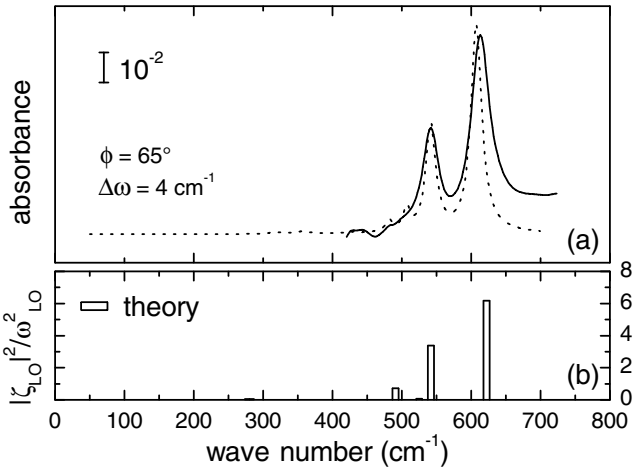

FIG. 2. (a) Grazing-incidence reflection-absorption spectrum of Lu_2O_3 on metal (solid). The resolution $\Delta\omega$ is shown in the panel. The dotted line is the spectral simulation. (b) Theoretical prediction of longitudinal optical modes energies and intensities.

reflection-absorption experiments, where the position of the spectral maxima slightly depends on the thickness of the film [13]. The LO energy loss function $-\mathrm{Im}(1/\varepsilon)$ is proportional to the SS in Fig. 2(a) [14]. We show in Fig. 2(b) the computed bulk LO frequencies and intensities.

We now focus on the static dielectric constant of lutetium oxide and discuss the microscopic origin of the lattice contribution ε_L. The data in Table I yield 8 and 7.80 for the experimental and theoretical ε_L, respectively, which further confirms the accuracy of the calculated spectrum. Similarly, the experimental $\varepsilon_{\infty} = 4$ agrees with the theoretical $\varepsilon_{\infty} = 4.18$. The experimental and theoretical estimates of ε_0 are hence 12 and 11.98, respectively, both in agreement with the value of 12 ± 1 extracted from capacitance-voltage curves in the 10–100 kHz range [3]. The main contributions to ε_L are due to TO8 and TO12, which involve almost exclusively polarization by O-atom displacement. Indeed, for all modes above TO7, we find $|\boldsymbol{\zeta}_j^{\mathrm{O}}|/|\boldsymbol{\zeta}_j^{\mathrm{Lu}}| > 10$, where $\boldsymbol{\zeta}_j^X$ is the partial mode-charge vector for atom X [5], i.e., the dipole moment contribution generated by the collective displacement of all atoms of species X in the jth normal mode. This can be seen in Fig. 3, which displays for all TO modes the modulus of the O and Lu partial mode-charge vectors $\boldsymbol{\zeta}_j^{\mathrm{O}}$ and $\boldsymbol{\zeta}_j^{\mathrm{Lu}}$ and of their sum $\boldsymbol{\zeta}_j = \boldsymbol{\zeta}_j^{\mathrm{O}} + \boldsymbol{\zeta}_j^{\mathrm{Lu}}$ (panel a). The angle α between $\boldsymbol{\zeta}_j^{\mathrm{O}}$ and $\boldsymbol{\zeta}_j^{\mathrm{Lu}}$ is displayed in panel b. All IR efficient modes are dominated by oxygen-related dipoles. Mixed or Lu-related modes at low frequencies are inefficient due to their small dipole moment and/or to the misalignment of the two contributions. On the basis of these results, we expect that ε_L should be similar for all bixbyite structure A_2O_3 if the mass ratio $m_{\mathrm{A}}/m_{\mathrm{O}}$ is sufficiently large. This appears to hold already for Y_2O_3 ($m_{\mathrm{Y}}/m_{\mathrm{O}} < 6$), whose TO IR spectrum [15] closely resembles Fig. 1(a).

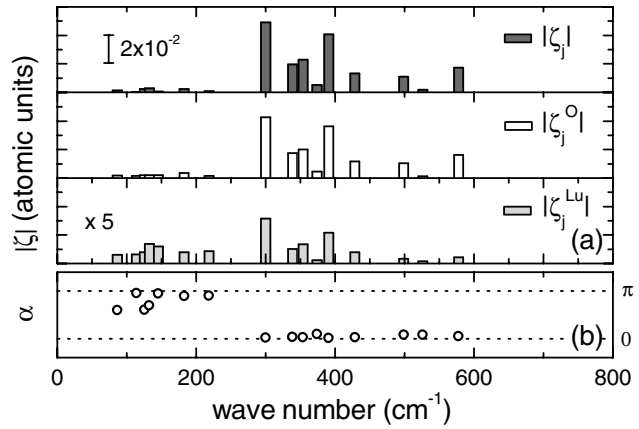

FIG. 3. (a) A comparison among total, O-related, and Lu-related transverse optical mode-charge vectors. All modes above about 300 cm^{-1} are mostly O related. (b) Angle α between Lu- and O-related partial mode-charge vectors. Small angles mean constructive composition of the vectors.

The value of ε_L of lutetia is not very high because of the large frequencies of the dominant IR modes and of the moderate dynamical charge anomaly (the average trace of the cation dynamical charge tensors is 3.65 versus nominal ionicity of 3). We note that, in the competing hexagonal structure (unstable for Lu_2O_3, but stable for, e.g., La_2O_3), the main IR modes are also oxygen dominated, but have lower frequencies, 220 cm^{-1} in plane and 260 cm^{-1} on axis, resulting in a larger ε_0, 20 in plane and 17 on axis. The average dynamical charges are very similar in the bixbyite and hexagonal phases, so we conclude that, in general, hexagonal A_2O_3 should have dielectric constants 1.5–2 times larger than bixbyite A_2O_3. The precise value depends on the dynamical charge tensor of the specific cation (preliminary results for La_2O_3 give a cation charge of 4.3).

In summary, in this Letter we presented a detailed analysis of the infrared dielectric function of a complex high-κ insulator, bixbyite Lu_2O_3. This joint experimental and theoretical work provides a detailed insight into the origin of the value of ε_0 in high-κ materials in general—i.e., of the very reason which makes this class of materials fundamental for current research-level and forthcoming production microelectronic devices. Experimental and theoretical results, in excellent mutual agreement, establish a robust link between lattice dynamics and dielectric properties in high-κ materials.

The authors thank C. Wiemer (MDM) for x-ray reflectivity and diffraction analyses. This work was funded by INFM through the PAIS project REOHK and Parallel Computing Initiative, and by the Italian Ministry of Foreign Affairs.

[1] *Alternative Gate Dielectrics for Microelectronics*, MRS Bulletin Vol. 27, edited by G. Wilk and R. M. Wallace (Material Research Society, Warrendale, 2002).

[2] G. D. Wilk, R. M. Wallace, and J. M. Anthony, J. Appl. Phys. **89**, 5243 (2001).

[3] G. Scarel, E. Bonera, C. Wiemer, G. Tallarida, S. Spiga, M. Fanciulli, I. L. Fedushkin, H. Schumann, Yu. Lebedinskii, and A. Zenkevich, Appl. Phys. Lett. **85**, 630 (2004).

[4] V. P. Tolstoy, I. V. Chernyshova, and V. A. Skryshevsky, *Handbook of Infrared Spectroscopy of Ultrathin Films* (John Wiley & Sons, Hoboken, 2003); Y. J. Chabal, Surf. Sci. Rep. **8**, 211 (1988).

[5] S. Baroni, P. Giannozzi, and A. Testa, Phys. Rev. Lett. **58**, 1861 (1987); S. Baroni, S. De Gironcoli, A. Dal Corso, and P. Giannozzi, Rev. Mod. Phys. **73**, 515 (2001); X. Gonze, Phys. Rev. B **55**, 10 337 (1997); X. Gonze and C. Lee, Phys. Rev. B **55**, 10 355 (1997).

[6] The ABINIT code (http://www.abinit.org) is a common project of the Université Catholique de Louvain, Corning Inc., and other contributors; see also X. Gonze *et al.*, Comput. Mater. Sci. **25**, 478 (2002).

[7] R. Wyckoff, *Crystal Structures* (John Wiley & Sons, New York, 1964), Vol. 2.

[8] K. Yamamoto and H. Ishida, Appl. Opt. **34**, 4177 (1995).

[9] W. N. Hansen, J. Opt. Soc. Am. **58**, 380 (1968).

[10] D. W. Berreman, Phys. Rev. **130**, 2193 (1963).

[11] V. M. Da Costa and L. B. Coleman, Phys. Rev. B **43**, 1903 (1991).

[12] The dielectric function of cobalt silicide is modeled following Z.-C. Wu, E. T. Arakawa, J. R. Jimenez, and L. J. Schowalter, J. Appl. Phys. **71**, 5601 (1992). For the energy range considered in this Letter the penetration depth $\lambda/4\mathrm{Im}(\varepsilon^{1/2})$ is smaller than the silicide thickness.

[13] Th. Scherübl and L. K. Thomas, Appl. Spectrosc. **51**, 844 (1997).

[14] The thickness of the film studied in this Letter is well below the Berreman thickness d_B,

$$d_B = \frac{\lambda}{2\pi}\frac{\cos\phi}{\sin^2\phi}\left[\mathrm{Im}\left(\frac{1}{\varepsilon}\right)\right]^{-1}_{\max},$$

a value indicating the upper limit for a linear relationship between the reflectance-absorbance and (i) the thickness of the film and (ii) the longitudinal energy loss function. See Refs. [4,11,13].

[15] J. J. Chambers and G. N. Parsons, J. Appl. Phys. **90**, 918 (2001).